HHS Public Access

Author manuscript

Arterioscler Thromb Vasc Biol. Author manuscript; available in PMC 2020 March 01.

Published in final edited form as:

Arterioscler Thromb Vasc Biol. 2019 March ; 39(3): 467–481. doi:10.1161/ATVBAHA.118.312233.

Disturbed flow increases UBE2C via loss of miR-483-3p, inducing aortic valve calcification by the HIF1α pathway in endothelial cells

Joan Fernandez Esmerats[1], **Nicolas Villa-Roel**[1], **Sandeep Kumar**[1], **Lina Gu**[1], **Md Tausif Salim**[2], **Michael Ohh**[3], **W. Robert Taylor**[1,4], **Robert M. Nerem**[5], **Ajit P. Yoganathan**[1,2], and **Hanjoong Jo**[1,4,†]

[1]Wallace H. Coulter Department of Biomedical Engineering at Georgia Institute of Technology and Emory University

[2]School of Chemical and Biomolecular Engineering, Georgia Institute of Technology

[3]Department of Biochemistry, Faculty of Medicine, University of Toronto, Toronto, CA

[4]Division of Cardiology, Department of Medicine, Emory University

[5]Parker H. Petit Institute for Bioengineering and Bioscience, Georgia Institute of Technology. Atlanta, GA, USA

Abstract

Objective: Calcific aortic valve disease (CAVD), characterized by aortic valve (AV) sclerosis and calcification, is a major cause of death in the aging population; however, there are no effective medical therapies other than valve replacement. AV calcification preferentially occurs on the fibrosa-side, exposed to disturbed flow (d-flow), while the ventricularis-side exposed to predominantly stable flow (s-flow) remains protected by unclear mechanisms. Here, we tested the role of novel flow-sensitive ubiquitin E2 ligase-C (UBE2C) and microRNA-483–3p (miR-483) in flow-dependent AV endothelial function and AV calcification.

Approach and Results: Human AV endothelial cells (HAVECs) and fresh porcine AV (PAV) leaflets were exposed to s-flow or d-flow. We found that UBE2C was upregulated by d-flow in HAVECs in the miR-483-dependent manner. UBE2C mediated OS-induced endothelial inflammation and endothelial-mesenchymal-transition (EndMT) by increasing the hypoxia-inducible factor1α (HIF1α) level. UBE2C increased HIF1α by ubiquitinating and degrading its upstream regulator von Hippel-Lindau (pVHL). These *in vitro* findings were corroborated by immunostaining studies using diseased human AV leaflets. Additionally, we found that reduction of miR-483 by d-flow led to increased UBE2C expression in HAVECs. The miR-483 mimic protected against endothelial inflammation and EndMT in HAVECs and calcification of PAV

[†]**Corresponding author**: Hanjoong Jo, PhD, John and Jan Portman Professor, Wallace H. Coulter Department of Biomedical Engineering, Department of Medicine, The Division of Cardiology, Emory University and Georgia Institute of Technology, 1760 Haygood Drive, Atlanta, GA 30322, hjo@emory.edu.

Disclosures

None.

The authors declare that all supporting data are available within the article and its online supplementary files.

leaflets by downregulating UBE2C. Moreover, treatment with the HIF1α inhibitor (PX478) significantly reduced PAV calcification in static and d-flow conditions.

Conclusions: These results suggest that miR-483 and UBE2C are novel flow-sensitive anti- and pro-CAVD molecules, respectively, that regulate the HIF1α pathway in AV. The miR-483 mimic and HIF1α pathway inhibitors may serve as potential therapeutics of CAVD.

Keywords

Flow; AV endothelial cells; Ubiquitination; Inflammation; EndMT; AV calcification; miR-483; UBE2C; pVHL; HIF1α

Introduction

Calcific Aortic Valve Disease (CAVD), characterized by aortic valve (AV) stenosis and insufficiency (regurgitation), is a major cause of cardiac-related deaths worldwide, especially in the aging population of advanced countries[1, 2]. Once developed, it is primarily treated through AV repair or replacement by surgical or transcatheter methods[3, 4]; however, there are currently no pharmacological treatment options available. CAVD is no longer considered a passive degenerative disease, but it is actively regulated via cellular and molecular pathways that lead to sclerosis (thickening and fibrosis) and calcific lesions[5–11]. AVs are a tri-layered structure composed of the fibrosa (in the aortic side), spongiosa (the middle layer) and ventricularis (facing the left ventricle). Endothelial cells (ECs), interstitial cells (VICs) and leukocytes are key cell types found in the AV and are actively regulated by genetic, biological pathways, and mechanical forces (e.g. shear and stretch)[8, 12]. Multiple pathogenic processes leading to CAVD have been identified: endothelial dysfunction, inflammation, EndMT, angiogenesis, apoptosis, extracellular matrix (ECM) remodeling, fibrosis and osteogenesis lead to sclerosis and calcification[12]. Endothelial dysfunction and inflammation are early events, which in turn lead to phenotypic switching of quiescent VICs to activated VICs and osteogenic VICs, resulting in AV sclerosis and calcification[7, 12–14]. Factors produced in AV ECs in response to various stimuli, including shear stress that promote inflammation, EndMT, pro-fibrotic and pro-calcific responses of VICs are emerging. Osteogenic mediators include bone morphogenic protein 2 and 4, alkaline phosphatase, TGF-β1, Runx2, osteopontin, osteonectin, matrix gla protein and tenascin C[5, 6, 15–17]. AV calcific nodules are composed of apoptotic cells and hydroxyapatite mineral and are surrounded by osteoblast-like cells and remodeled ECM[18].

Interestingly, AV disease occurs in a side-specific manner. The fibrosa side is exposed to disturbed flow (d-flow), characterized by low magnitude and oscillatory shear stress [oscillatory shear index (OSI) ~>0.25][19], and is preferentially calcified. In contrast, the ventricularis side is exposed mostly to stable flow (s-flow), characterized by high magnitude, uni-directional, and pulsatile shear stress [OSI ~<0.1][19], and is often protected from calcification[1, 6]. The side-specific AV calcification is hypothesized to be due to endothelial dysfunction in response to d-flow in the fibrosa, while anti-inflammatory and anti-calcific responses prevail in the ventricularis side exposed to a more favorable flow condition [20, 21]. AV leaflets respond to various flow conditions mimicking d-flow and s-flow in a manner consistent to the *in vivo* conditions. For example, exposure of porcine AV leaflets *ex vivo* to

d-flow increases matrix proteinase activities[22], stimulates ECM remodeling[23], and increases AV calcification[23] in comparison to the s-flow. In the case of arteries, d-flow leads to atherosclerosis by regulating flow-sensitive genes and proteins in endothelial cells, which leads to endothelial dysfunction and pro-atherogenic pathways[24–26]. However, it is less clear which flow-sensitive genes and proteins in the AV regulate CAVD.

To identify flow-sensitive and side-specific genes, we previously conducted gene (mRNA) and microRNA (miRNA) microarray studies using human AV ECs exposed to unidirectional laminar flow (s-flow) or oscillating flow (d-flow) as well as in porcine AV leaflets[23, 27, 28]. The roles of these flow-sensitive miRNAs in AV biology and disease are beginning to emerge but are far from clear. Recently, we showed that miR-214 and miR-181b expression is upregulated by d-flow in HAVECs and in the porcine AV fibrosa[23, 28]. We further showed that exposure of porcine AV leaflets to d-flow increased miR-214, which regulated TGF-β expression with moderate effect on collagen production but no effect on AV calcification[23]. We also found that OS-induced miR-181b regulated matrix metalloproteinase activity in part by targeting the tissue inhibitor of metalloproteinases-3 in HAVECs, but its effect on AV calcification is still unclear[28].

In this study, we investigated miR-483 because our gene array data indicated that it might be a flow-sensitive miRNA in HAVECs. Recently, miR-483 has been shown to target the connective tissue growth factor (CTGF), which mediates EndMT in human umbilical vein ECs[29]. In another study using vascular smooth muscle cells and heart tissue samples, angiotensin II reduced expression of miR-483, which was shown to target four members of the renin-angiotensin system: AGT, ACE-1, ACE-2 and AGTR2[30]; however, the role of miR-483 in HAVEC biology and CAVD is still unknown.

Here, we found that UBE2C is a major target of miR-483[31]. UBE2C, also known as UBCH10, is an E2 ubiquitin conjugating enzyme. While overexpression of UBE2C is well documented in various cancer cells[32–36], its role in endothelial function and CAVD is yet to be determined. Ubiquitination is upregulated in calcified valves[37], but its underlying mechanisms and whether it plays any role in AV calcification or endothelial function is unknown. Interestingly, Hypoxia-inducible factor 1-α (HIF1α) expression, which is controlled by Von Hippel Lindau protein (pVHL)[38–41], is upregulated by d-flow conditions in vascular ECs and atherosclerotic conditions[42]. UBE2C is a member of the Anaphase Promoting Complex/Cyclosome (APC/C), which is also known to bind to pVHL[43]. Therefore, we hypothesize that UBE2C would regulate the HIF1α pathway by controlling pVHL.

Here, we show the novel mechanism by which the miR-483 target, UBE2C, regulates the pVHL and HIF1α pathway, leading to endothelial inflammation, EndMT, and subsequent AV calcification. We also show evidence suggesting that miR-483 mimic and HIF1α inhibitors may serve as potential therapeutics to reduce CAVD.

Methods

Cell culture and *in vitro* flow system

HAVECs were isolated from noncalcified AVs obtained from transplant recipient hearts (n = 6) following the Institutional Review Board-approved protocol at Emory University as we have previously described[27]. Patient characteristics used for HAVEC isolations as well as the detailed cell purity characterizations were described in detail in our previous publication[44]. For the majority of our flow experiments, we exposed confluent cells to steady unidirectional flow (s-flow, 20 dyn/cm^2) or bidirectional oscillatory flow (d-flow, ±5dyn/cm^2 at 1Hz) to mimic the ventricularis- and fibrosa-side flow, respectively, using the cone-and-plate viscometer for 24 hour experiments, as we reported[45, 46]. Briefly, a cone controlled by a motor is placed in a standard 10cm tissue culture dish containing confluent HAVEC monolayer. The cone was rotated uni-directionally or bi-directionally at different velocities to generate s-flow and d-flow conditions, respectively. Under these conditions, s-flow induces anti-inflammatory KLF2 expression and d-flow generates inflammatory signaling at levels like those observed *in vivo*[27]. For some studies, we used the Ibidi flow channel system (Ibidi, Munich, Germany) to expose HAVECs to >72 hours of shear to maintain sterility throughout the chronic studies that require media change. The Ibidi shear system was set up per the company's instructions and proprietary software was used to control the level of shear applied to cells by controlling total media flow rate through the channels of known dimensions.

Human Embryonic Kidney (HEK) cells were purchased from ATCC (CRL-1573) and cultured in DMEM (VWR Scientific 45000–332 4.6g/L glucose), 10% FBS (Atlanta Biologicals S11550), 1% L-Glutamine (Thermo Fisher Scientific 25030–081) and 1% Penicillin Streptomycin (Life Technologies 15140122).

Porcine AV tissue harvest and *ex vivo* shear experiment

Hearts were obtained from healthy, female, non-pregnant pigs (aged 6 to 12 months) immediately after slaughter from a local abattoir (Holifield Farms, Covington, GA). The abattoir handles nearly exclusively female pigs due to an undesirable meat quality of male pigs for human consumption. The AV leaflets were immediately excised and thoroughly rinsed in sterile, nuclease-free HBSS at 4 °C. These excised leaflets were then placed in either RNAlater (Thermo Fisher Scientific AM7020; for generation of miRNA samples) or HBSS at 4 °C (VWR Scientific 45000–462; therapeutic studies). Valves were placed on ice and transported back to the laboratory. Upon arrival in the laboratory, dissected AVs were transferred to sterile HBSS at 4 °C under the sterile laminar flow hood and processed accordingly. Endothelial enriched RNA was obtained as previously described[27]. For static calcification studies, leaflets were placed under osteogenic media. Osteogenic media is composed regular DMEM (VWR Scientific 45000–332) supplemented with 1 mM glycerophosphate (Sigma Aldrich G9422), 10 μM dexamethasone (Sigma Aldrich D4902), 3.8 mM PO_4^{3-} (Fisher Scientific S374), and 1 ng/ml transforming growth factor (TGF-β 1, Sigma Aldrich t5050). This media has been shown to induce accelerated calcification in porcine AVs[47]. Tissues were transfected and media were changed at the start of the experiment and every 3 days for up to 14 days. To study the effect of flow on porcine AV

leaflets, the cone-and-plate bioreactor was used as we previously described[23, 48, 49]. AV leaflets were exposed to the fibrosa- or ventricularis-flow[48, 50] in the osteogenic media for 7 days (Fig. XIVa). Media were changed every three days and the entire setup was placed in a 5% CO2 incubator at 37°C.

Quantitative real-time PCR (qPCR)

Total RNA was isolated using miRNeasy Mini Kit (Qiagen 217004) and reverse transcribed for use in a two-step quantitative reverse transcribed–PCR using a qRT-PCR kits (Applied biosystems 4368814). For measurement of mRNA targets, qPCR was performed on selected genes using VeriQuest Fast SYBR QPCR Master Mix (Affymetrix 75690) with custom designed primers using 18S as house-keeping control. The PCR conditions were 2 min at 50 °C, 5 min at 95 °C, followed by 40 cycles of 95 °C for 4 s and 60 °C for 30 s. Fold changes between s-flow and d-flow were determined for all targets using the ΔΔCt method.

Mature miRNA assays were performed using miRNA quantification and was performed by SYBR green qPCR assay using miScript reverse transcription kit (Qiagen 218161) according to the manufacturer's instructions. qPCR was performed using VeriQuest Fast SYBR QPCR Master Mix (Affymetrix 75690) with miScript universal primer (Qiagen MS00033740) and the miRNA-specific forward primers and relative fold change was calculated. The specific mature primers were purchased from Qiagen. The amplification profile was denaturation at 95 °C, 15 min, followed by 40 cycles of 94 °C, 15 s; 55 °C, 30 s; and 70 °C, 30 s.

Monocyte adhesion assay

Monocyte binding was determined under using THP-1 monocytes (ATCC TIB-202). Briefly, THP-1 cells (1.5×10^5 cells/ml) were labeled with a fluorescent dye 2-,7-bis(carboxyethyl)-5 (6)-carboxyfluorescein-AM (BCECF; Thermo Fisher Scientific B1150) (1 mg/ml) in serum free RPMI medium (Thermo Fisher Scientific 11875093) for 45 min at 37 °C. Following exposure to flow or transfection treatments, the endothelial cells were washed in RPMI medium before adding BCECF-loaded THP-1 cells. After a 30-min incubation at 37 °C under no-flow conditions, unbound monocytes were removed by washing the endothelial dishes five times with HBSS and cells with bound monocytes were fixed with 4% Paraformaldehyde (Sigma Aldrich 47608) for 10 minutes. Bound monocytes were quantified by counting the cells under a fluorescent microscope.

Immunofluorescent staining of human AV tissues

Human AVs were obtained immediately following valve replacement surgeries in 16 patients at Emory University Hospital Midtown according to the IRB-approved study at Emory University with written informed consent. We previously reported the detailed patient demographics of this cohort used for this study[44]. Briefly, fifteen patients had trileaflet valves, while one patient had a bicuspid AV. Average age was 66 years old with 44% female, 12.5% diabetic patients, 38% dyslipidemic patients, and 75% hypertensive patients. Immediately following harvesting, the AVs were photographed, washed in ice-cold phosphate buffered saline, and cusps were individually snap-frozen in optimal cutting temperature (O.C.T.) compound (Tissue-Tek 23–730-571). Valves were then sectioned (8

μm) in the radial direction to include the base and free edge (tip), stored at −80°C and used for immunohistochemical staining studies.

Staining was performed as we have described previously[44], using specific antibody against UBE2C (Protein Tech 12134–2-AP), pVHL (Thermo Fisher Scientific PA5–27322), HIF1α (Bethyl laboratories A300–286A), CD31 (Abcam, ab9498), TWIST1 (EMD Millipore ABD29), RUNX2 (Santa Cruz Biotechnology SC10758) or VCAM1 (Abcam, ab134047) and appropriate secondary antibody conjugated to fluorophore at Alexa 488 or Alexa 568 (Life Technologies A11004 or A11011). Hoechst 33342 (Life Technologies H3570) was used to stain nuclei. All measurements were performed using ImageJ (NIH) and were represented as staining intensity normalized to DAPI intensity.

Transient transfection with oligonucleotides or plasmid

For the functional tests of miR-483 *in vitro* and *ex vivo,* cells or porcine AV leaflets were transiently transfected with miRNA-483 mimic (Exiqon 472350–001), non-targeting miR-mimic control (Qiagen YM00479902-ADA), anti-miR-483 (Exiqon 4100225), mismatched anti-miR control (Exiqon 4101427–102), siRNA control (Dharmacon D-001810–10-20), siRNA UBE2C (Dharmacon L-004693–00-0005), siRNA pVHL (Dharmacon L-003936–00-0005) or siRNA HIF1α (Exiqon 500100) using Oligofectamine (Invitrogen 12252011), as we described previously[51]. For static conditions, cells were lysed 48h after the transfection for RNA or protein assays. For flow experiments using the cone-and-plate system, HAVECs were first transfected for 24h, then exposed to flow for another 24h. For flow experiments using Ibidi system that requires a longer time (~72h) to align, transfected HAVECs were exposed to flow for another 72h. For *ex vivo* studies, AV leaflets were transfected every 72 hours when the tissues received fresh media. Following flow exposure, cells were lysed for RNA or protein assays.

For plasmid transfections, Lipofectamine 3000 (Thermo Fisher Scientific 15338030) was used as transfection reagent following manufacturers' protocol. The plasmids used were: pCMV6-UBE2C Myc-DDK-tagged (Origene technologies, RC208741), RpCMV-DsRed-Express2 (RFP, SnapGene pIRES2 DsRed-Express 2), pRc-CMV-HA-pVHL-WT, HA-pVHL-RRR, HA-pVHL-KRR, HA-pVHL-RKR and HA-pVHL-RRK[52, 53].

Immunoprecipitation studies

For pVHL or ubiquitin immunoprecitations, 25 μl of goat-Anti-Rabbit IgG (New England Biolabs, S1432S) or goat-Anti-Mouse IgG (New England Biolabs, S1431S) magnetic beads were pre-incubated (2 hour at RT) with 5 μg of anti-VHL antibody (Thermo Fisher Scientific PA5–27322) or an anti-total-ubiquitin antibody (Abcam ab128424). Cells were lysed using an IP lysis buffer (Thermo Fisher Scientific 87787) and added to the magnetic beads overnight at 4C. The magnetic beads were then washed five times with a Tris-EDTA buffer to remove non-bound proteins and the bound proteins were separated from the beads by adding SDS buffer and boiling the protein for 5 min. Immunoprecipitated samples were subjected to standard SDS-PAGE and Western blot. For HA-tag immunoprecitations, an Anti-HA immunoprecipitation kit (Sigma-Aldrich IP0010) was used per the manufacturer's

instruction. Immunoprecipitated samples were subjected to SDS-PAGE and Western blot as described above.

Cell proliferation

After treatment, cells were fixed with 4% Formaldehyde and stained for KI-67 (Abcam ab15580) and DAPI. Cells were quantified using ImageJ for both KI-67 positive cells and normalized to number of DAPI cells[54].

Cell cycle

After treatment, cells were detached from culture dish using trypsin, washed twice in HBSS with 2%FBS (centrifuged at 1000g for 5 mins) and fixed with 70% ice-cold ethanol added dropwise while gently vortexing. Cells were then washed twice with HBSS (centrifuged at 1250g for 5 mins). Finally, a solution of PI stain (50ug/mL, Invitrogen P1304MP) with RNAse A (0.5ug/mL, Qiagen 19101) was added to the cells for 15 mins prior to analysis using flow cytometry. Data was analyzed using FlowJo software[54].

Apoptosis Tunel staining

After treatment, cells were fixed with 4% Formaldehyde and apoptosis was quantified using an *in situ* Cell Death Detection Kit from Roche (Roche cat. # 11684795910) using the provided protocol. Cells were quantified microscopically using ImageJ[50].

Cell migration

After treatment, cell monolayers were scratched with a 200-μL pipette tip. The monolayer was washed once and the medium was replaced with 2% FBS media. Cells were quantified every two hours and the cell velocity was calculated using ImageJ[55].

Preparation of whole-cell lysate and immunoblotting

Following treatment, cells were washed three times with ice-cold HBSS and lysed with RIPA buffer (Boston Bioproducts BP-421). The protein content of each sample was determined by Pierce BCA protein assay. Aliquots of cell lysate were resolved by size on 10–12% SDS–polyacrylamide gels and subsequently transferred to a polyvinylidene difluoride membrane (Millipore). The membrane was incubated with the following antibodies: UBE2C (Protein Tech 12134–2-AP), Ubiquitin (Santa Cruz Technologies, sc-8017), HA-tag (Sigma-Aldrich 11867423001), pVHL (Thermo Fisher Scientic PA5–27322), GAPDH (Santa Cruz Biotechnology, sc-25778) or β-Actin (Sigma Aldrich, A5316) overnight at 4 °C at the concentration recommended by the manufacturer, followed by secondary antibody (Santa Cruz Biotechnology, 1:5000) for 1 h at RT. Protein expression was detected by a chemiluminescence method.

Statistical analysis

Statistical analyses were performed using GraphPad Prism software. All of the n numbers represent biological replicates. When technical replicates or triplicates were performed, those values were averaged and used as one biological data point. Error bars depict the standard error of the means. Initially, the datasets were analyzed for normality using the

Shapiro-Wilk test ($P<0.05$) and equal variance using the F test ($P>0.05$). Data that followed a normal distribution and possessed equal variance were analyzed using 2-tailed Student's t test or one-way ANOVA, where appropriate with Bonferroni Post-Hoc test as needed. In the case where the data showed unequal variances, an unpaired t-test with Welch's correction was performed or Brown-Forsythe and Welch ANOVA for multiple comparisons. In the case where the data failed the Shapiro-Wilk test ($P>0.05$), a non-parametric Mann-Whitney U test was conducted for pairwise comparisons or the Kruskal-Wallis for multiple groups was performed. For human AV staining studies, we conducted one sample t-test if the data followed a normal distribution else a Wilcoxon signed-rank test was performed. A $P<0.05$ was considered statistically significant.

Results

miR-483 expression is shear-sensitive and side-specific, and it inhibits shear-induced EndMT and endothelial inflammation

In our previous microRNA array study using HAVECs, miR-483 appeared to be a shear-sensitive miRNA[27], but its function was unknown. To confirm this, we validated the shear-sensitivity of miR-483 by qPCR in HAVECs. Subjecting HAVECs to d-flow conditions for 24 hours decreased miR-483 expression by 63% compared to the s-flow condition (Fig. 1a). Additionally, we found that miR-483 level in static condition was similar to the d-flow conditions (Fig. Ia). To determine whether miR-483 is expressed in a side-specific manner in AVs, endothelial-enriched RNAs were collected from healthy porcine AVs and miR-483 expression was quantified by qPCR. Endothelial purity levels of these RNA preparations were assessed by measuring markers of macrophages (CD11b), endothelial cells (PECAM1), and VICs (α-SMA) by qPCR. Consistent to our previous report where we developed our endothelial-enriched RNA preparation method[23], our endothelial-enriched RNA preparations used in this study showed an abundant level of PECAM1 while the levels of CD11b and α-SMA were barely detectable (Fig. II). The level of miR-483 was 45% lower in the fibrosa side (naturally exposed to d-flow conditions) compared to the ventricularis side (naturally exposed to pulsatile, s-flow conditions) (Fig. 1b). These results showed that miR-483 expression is reduced by d-flow in HAVECs and in the fibrosa-side where the AV leaflets are exposed to d-flow.

Next, we determined the role of miR-483 in shear-dependent responses of HAVECs by using miR-483 mimic (to overexpress miR-483) or anti-miR-483 (to silence miR-483). HAVECs were treated with miR-483 mimic (20 nM increased miR-483 level by ~200-fold) or anti-miR-483 (50nM reduced miR-483 level by 80%) for 24 hours (Fig. Ib-d), followed by d-flow or s-flow for 24 hours, respectively. D-flow exposure significantly increased expression of EndMT markers (*TWIST1, TRANSGELIN (TAGLN), SNAIL and SLUG)* (Fig. 1c), which was significantly reduced by treatment with miR-483-mimic in HAVECs. We also tested other markers of EndMT such as *CALPONIN, α-SMA, and VE-CADHERIN* and even though they showed a trend they were not significant, so we decided not to study them further. In contrast, anti-miR-483 treatment dramatically increased EndMT markers under the s-flow condition in HAVECs (Fig. 1d), suggesting a major role of miR-483 in shear-sensitive EndMT.

Next, we tested whether miR-483 regulates OS-induced endothelial inflammation as determined by monocyte adhesion and expression of pro-inflammatory marker genes (*IL6, ICAM1 and VCAM1*) (Fig. 1e-g), while using *KLF2* (a well-known s-flow-induced anti-inflammatory gene) as a control. Compared to s-flow, d-flow-induced endothelial inflammation was significantly reduced by miR-483-mimic. In contrast, silencing miR-483 by anti-miR-483 significantly induced endothelial inflammation under the s-flow condition, suggesting the role of miR-483 in flow-dependent endothelial inflammation. Interestingly, neither miR-483-mimic nor anti-miR-483 affected KLF2 expression level (Fig. 1f and g), suggesting that KLF2 is not a downstream mediator of the miR-483 effect. The anti-inflammatory effect of miR-483 was also confirmed in HAVECs in static (no-flow) conditions (Fig. III). In addition, miR-483-mimic treatment inhibited proliferation of HAVECs, while anti-miR-483 increased proliferation (Fig. IVa). On the other hand, miR-483 mimic showed no effect on apoptosis, whereas anti-miR-483 induced apoptosis by 2-fold compared to control (Fig. IVb). Lastly, miR-483 modulation showed no significant effect on cell migration or cell cycle (Fig. IVc-d). Together, these results showed that reduction in miR-483 level under d-flow condition leads to endothelial inflammation and EndMT, which are well known to be critical for CAVD pathogenesis[6–11, 56].

UBE2C is a flow-sensitive and side-specific target of miR-483 in HAVECs and in human AVs

To determine the mechanisms by which miR-483 mediates flow-dependent effects on HAVEC function, we identified potential targets of miR-483. To this end, we conducted an *in silico* analysis comparing the predicted targets of miR-483 (950 predicted genes by the miRWalk and miRTarBase databases) with OS-induced genes (239 genes) from our previous HAVEC transcriptome array study[27] (Fig. Va). This *in silico* analysis revealed nine genes that were predicted gene targets of miR-483 and flow-sensitive genes in our HAVEC transcriptome microarray: *ABCB9, ASH2L, DHX33, GADD45B, PSAT1, PSEN2, TMEM88, TOMM20, and UBE2C* (Fig. Vb). To determine whether they are also flow-sensitive, HAVECs were exposed to s-flow or d-flow for 24 hours and the expression of these 9 genes was tested by qPCR. This study indicated that d-flow increased 6 of these 9 genes (Fig. Vb). We next determined which of these six flow-sensitive genes were significantly regulated by miR-483 using the miR-483-mimic or anti-miR-483. The results showed that *ASH2L*, *UBE2C* and *PSAT1* were consistently regulated by the miR-483 modifications in static HAVECs (Fig. Vc and d). We further validated if the flow-sensitive expressions of *ASH2L*, *UBE2C* and *PSAT1* were mediated by miR-483 following treatment of HAVECs with miR-483 mimic under the d-flow condition or anti-miR-483 under the s-flow condition. *ASH2L* and *UBE2C* were regulated by miR-483 under flow conditions, but PSAT1 was not (Fig. Ve and f). These results demonstrate that ASH2L and UBE2C are flow-sensitive targets of miR-483. Interestingly, knockdown of UBE2C alone dramatically prevented OS-induced endothelial inflammation (as discussed below in Fig. 2h), demonstrating its dominant role. Although both UBE2C and ASH2L are likely to play major roles in CAVD, they are involved in potentially two very complex and different pathways (UBE2C on ubiquitin-dependent pathways and ASH2L on epigenetic regulation through histone modifications) and studying both simultaneously would interfere with focused studies; therefore, we decided to concentrate on UBE2C.

At the protein level, d-flow exposure significantly increased UBE2C expression compared to the s-flow condition in HAVECs (Fig. 2a and b). In addition, the OS-induced increase in UBE2C expression was significantly blocked by miR-483 mimic in HAVECs (Fig. 2c and d), further validating that the reduction of miR-483 by d-flow leads to de-repression of UBE2C expression. Similar results were observed in static conditions (Fig. Vg and h). Moreover, miR-483 was previously shown to directly bind to the 3'UTR of UBE2C[31].

UBE2C regulates OS- and miR-483-dependent inflammation and EndMT in HAVECs.

We next tested whether UBE2C mediates endothelial inflammation and EndMT by treating HAVECs with UBE2C siRNA (siUBE2C), anti-miR-483 or a combination of both. SiRNA-mediated knockdown of UBE2C inhibited endothelial inflammation in static basal condition as well as in response to anti-miR-483 (to increase UBE2C expression) (Fig. 2e and f). This result suggests that UBE2C mediates the endothelial inflammation induced by the loss of miR-483. We also found that overexpression of UBE2C using the plasmids dose-dependently increased monocyte adhesion in HAVECs (Fig. 2g), further supporting our hypothesis that UBE2C induces pro-inflammatory responses in HAVECs.

Furthermore, we tested if OS-induced pro-inflammatory and pro-EndMT responses could be reverted by knockdown of UBE2C using siUBE2C. UBE2C knockdown prevented OS-induced monocyte adhesion and induction of the pro-inflammatory markers (*VCAM1* and *ICAM1*) without affecting *KLF2* or *ASH2L* expression in HAVECs (Fig. 2h and i). Moreover, siUBE2C treatment significantly reduced several markers of EndMT (*TWIST1, TAGLN and SLUG*) (Fig. 2j). In addition, siUBE2C decreased cell proliferation, but not cell migration in HAVECs. (Fig. VI). Moreover, knockdown of UBE2C with SiUBE2C in HAVECs did not alter miR-483 levels, suggesting that UBE2C is not an upstream regulator of miR-483 (Fig. VIc). Together, these results showed that UBE2C is indeed a key miR-483 target gene, which plays a dominant role in OS-induced pro-inflammatory and pro-EndMT responses in HAVECs.

UBE2C mediates flow-sensitive expression of pVHL and HIF1α.

Here, we hypothesized that the increase in UBE2C (due to the loss of miR-483 under the d-flow condition) leads to ubiquitination and degradation of pVHL, which in turn increases HIF1α levels, leading to increased expression of its target genes, endothelial inflammation and EndMT (Fig. 3a). First, we found that the expression of pVHL and HIF1α were highly flow-sensitive, but inversely regulated in HAVECs. Under s-flow exposure for 72 hours, expression of pVHL was high, while HIF1α expression was undetectable. In contrast, under OS, pVHL was low while HIF1α was high at the protein and mRNA levels (Fig. 3b-d and Fig. VII). We found that UBE2C silencing significantly increased pVHL expression while preventing HIF1α induction under the d-flow condition (Fig. 3e-h and Fig. VIII), demonstrating that UBE2C regulates flow-dependent expression of pVHL and HIF1α.

Next, we tested whether the flow-dependent changes in expression of UBE2C, pVHL, and HIF1α observed in HAVECs *in vitro* also occur in diseased human AV leaflets. We hypothesized that those molecules such as UBE2C, HIF1α, and markers of inflammation, EndMT and calcification are overexpressed in the fibrosa side exposed to d-flow (d-flow).

To this end, we carried out immunohistochemical staining study using human AV tissue samples obtained from patients who underwent AV repair surgery as described in the Method and as previously reported by us[44]. UBE2C and HIF1α expression was significantly higher in the fibrosa-side of the human AV leaflets, whereas pVHL expression was higher in the ventricularis-side (Fig. 3i and j). Furthermore, markers of inflammation (VCAM1), EndMT (TWIST1), and calcification (RUNX2) (Fig. 3i and j) were highly expressed in the fibrosa side demonstrating side-dependent expression of pro-CAVD markers. As a control, endothelial marker CD31 was used to show intact endothelial layers in these AVs (Fig. IXa). Similar results were also obtained in porcine AVs (Fig. IXb-e). These staining results clearly corroborate the side-dependent expression of UBE2C, pVHL, and HIF1α, with markers of inflammation, EndMT, and calcification in the fibrosa side of human AV leaflets.

UBE2C binds and ubiquitinates pVHL, leading to its degradation.

We next examined how UBE2C (a E2 ubiquitin ligase) regulates pVHL expression. Although UBE2C is a member of APC/C complex, which is known to bind and ubiquitinate pVHL for proteasomal degradation[43], it was unknown whether UBE2C can mediate pVHL ubiquitination. Therefore, we tested whether UBE2C mediates pVHL expression in an ubiquitination-dependent manner. To this end, HAVECs were transfected with siUBE2C, and ubiquitinated proteins were pulled down and western blotted using a pVHL antibody. We found that knockdown of UBE2C decreased ubiquitinated pVHL levels in the immunoprecipitates (Fig. 4a). This result was independently validated by immunoprecipitating pVHL first, followed by ubiquitin western blotting, demonstrating that ubiquitination of pVHL was reduced when UBE2C was knocked down in HAVECs (Fig. 4b). As expected, levels of pVHL in these cell lysates were increased (Fig. Xa and b).

Since UBE2C has never been shown to bind and ubiquitinate pVHL, we tested whether they associate with each other by co-transfecting HEK cells with plasmids overexpressing UBE2C or RFP as a control and HA-pVHL-WT or HA-pVHL-RRR mutant. The HA-pVHL-RRR mutant has its three Lys ubiquitination sites (K159, K171 and K196) modified to Arg so that they cannot be ubiquitinated[52, 53]. We used HA-tag antibody to immunoprecipitate HA-pVHL-WT and HA-pVHL-RRR (Fig. 4c). UBE2C co-immunoprecipitated with either HA-pVHL-WT or HA-pVHL-RRR (Fig. 4c and Fig. Xc). Interestingly, the pVHL Western blot of HA-pVHL immunoprecipitates showed bands at ~28, 34, 55, 80 kDa, potentially representing poly-ubiquitinated pVHLs in a manner dependent on UBE2C and pVHL-ubiquitination sites (Fig. 4c). Furthermore, the Western blot using the ubiquitin antibody for the HA-pVHL immunoprecipitates showed ubiquitinated proteins at ~35, 40, 85, 100 kDa in a manner dependent on UBE2C and pVHL-ubiquitination sites (Fig. Xd).

Next, we tested whether UBE2C regulates pVHL levels in a ubiquitination-dependent manner by co-transfecting HEK cells with plasmids overexpressing UBE2C or RFP control and HA-pVHL WT or mutants. Four different HA-pVHL double or triple mutants on the three Lys ubiquitination sites were used (RRR, KRR, RKR, and RRK) in comparison to WT[52, 53]. Expression of pVHL-WT and the three pVHL double mutants, but not the RRR triple mutant was decreased as UBE2C expression increased in a dose-dependent manner

(Fig. 4d-g and Fig. XI). This result clearly demonstrates that pVHL degradation is UBE2C-dependent and it requires at least one of the three Lys ubiquitination sites. These results also demonstrate that UBE2C binds to pVHL and mediates its degradation by the ubiquitination-dependent manner.

pVHL and HIF1α mediate UBE2C-dependent inflammation and EndMT in HAVECs.

We tested whether pVHL and HIF1α regulate endothelial inflammation and EndMT by using sipVHL or siHIF1α in HAVECs. Knockdown of pVHL increased monocyte adhesion (Fig. 5a) as well as markers of inflammation and EndMT (Fig. 5b). We also found that knockdown of pVHL did not affect *HIF1α* mRNA levels. This was expected (Fig. 5b) as pVHL is known to regulate HIF1α protein levels via ubiquitination and proteasome degradation[38, 57]. In contrast, knockdown of HIF1α inhibited monocyte adhesion (Fig. 5c) and markers of inflammation and EndMT, while not affecting pVHL levels (Fig. 5d). We then tested whether UBE2C-induced endothelial inflammation and EndMT is mediated by either pVHL or HIF1α, using siUBE2C, sipVHL or siHIF1α in combination. Knockdown of both, UBE2C and pVHL, induced endothelial inflammation and EndMT (Fig. 5e and f). In contrast, silencing of both, UBE2C and HIF1α, inhibited inflammation and EndMT (Fig. 5e and f). These results suggest that endothelial inflammation and EndMT, induced by UBE2C, is mediated by pVHL and HIF1α in HAVECs.

MiR-483 mimic and HIF1α chemical inhibitor PX478 inhibit calcification in porcine aortic valves

Next, we tested whether the flow-dependent miR-483, UBE2C, pVHL and HIF1α pathway plays a significant role in CAVD. To this end, miR-483 mimic and the HIF1α inhibitor PX478 were selected as treatments. We cultured freshly obtained healthy porcine AV leaflets in osteogenic media[47] for 14 days to induce calcification (Fig. 6a). Treatment with the miR-483 mimic (20nM every three days) significantly inhibited AV calcification as measured by Alizarin Red staining (Fig. 6b and c and Fig. XIIa) and Arsenazo assay (Fig. 6d). The anti-calcific effect of miR-483 was mediated by decreasing UBE2C and HIF1α while upregulating pVHL (Fig. 6e and f). Treatment with PX478 (20μM every three days) showed a dramatic inhibition of AV calcification (Fig. 6g-i and XIIb) and significantly decreased HIF1α expression (Fig. XIII). More importantly, we tested whether PX478 can inhibit AV calcification under the flow condition mimicking disturbed fibrosa-flow. Porcine AV leaflets to fibrosa-flow (Fib.) or ventricularis-flow (Ven.) conditions (Fig. XIVa) using the pro-osteogenic media with PX478 (20 μM) or vehicle for 7 days. As we previously reported using the same *ex vivo* flow device[23], fibrosa-flow increased AV calcification by 52% above that of the ventricularis-flow. Moreover, treatment of porcine AV leaflets with PX478 under the fibrosa-flow condition significantly inhibited AV calcification to the level of the ventricularis-flow (Fig. 6j). These results demonstrate the therapeutic potential of targeting miR-483 and the HIF1α pathway in treatment of CAVD.

Discussion

The main findings of our study are that miR-483 is a novel flow-sensitive and side-dependent miRNA that regulates endothelial inflammation and EndMT by targeting UBE2C,

which in turn regulates pVHL and HIF1α under normal atmospheric conditions, ultimately leading to AV calcification. We also found that miR-483 mimic as well as the HIF1α inhibitor PX478 effectively reduced AV calcification of porcine AVs *ex vivo*.

We found that miR-483 expression is increased by s-flow and in the ventricularis-side which is exposed to s-flow, while decreased by d-flow and in the fibrosa-side which is exposed to d-flow. Most flow experiments carried out in this study used the simplified s-flow and d-flow conditions for technical reasons to represent the more complex *in vivo* ventricularis and fibrosa flow profiles, respectively (Fig. XIVa). However, to validate whether the simplified s-flow and d-flow induced EC responses similar to that in response to the more complex flow profiles, we improved our flow application method and carried out additional studies by exposing HAVECs to the more complex, *in vivo* ventricularis and fibrosa flow profiles. As shown in Fig. XIV, the stable ventricularis flow aligned HAVECs, upregulated KLF2 and miR-483, and downregulated UBE2C, ICAM1 and IL6 as shown in response to s-flow (Figs. 1, 2, V and XV). This supports that HAVECs respond similarly to both the simplified flow conditions and the more realistic complex flow conditions tested. Therefore, we continued to use simplified s-flow and d-flow conditions for the rest of the studies for the technical convenience.

Our results demonstrated that miR-483 potently regulates endothelial function by protecting against inflammation, proliferation, and EndMT. The role of miR-483 was reported mostly in cancer cells where it regulates proliferation[58, 59] and apoptosis[58, 60, 61]; however, the role of miR-483 is still unclear in the cardiovascular system. Recent data showed that miR-483 mediates EndMT by targeting CTGF in human umbilical vein ECs[29]. Angiotensin II was shown to inhibit expression of miR-483 targeting the renin-angiotensin system genes in smooth muscles and heart[30]. These genes including CTGF, however, were not flow-sensitive in our gene array study using HAVECs and porcine AVs[27, 62]; therefore, we did not study them. MiR-483 is located in the intronic region of insulin-like growth factor 2 (IGF2), and it was shown to be mediated by KLF4[29]. Similarly, we found that expression of miR-483 and IGF2 were mediated in a KLF2-dependent manner in HAVECs (Fig. XV).

We have identified UBE2C as a flow-sensitive target of miR-483 through our *in silico* and validation studies. UBE2C is a member of the APC/C complex and is known to catalyze the initial mono-ubiquitination of protein substrates such as cyclins[63–65]. Once cyclins are mono-ubiquitinated, another E2 ligase, Ube2s, then elongates the ubiquitin chain (poly-ubiquitination) leading to their proteasomal degradation[66, 67]. Interestingly, pVHL is another well-known substrate of both APC/C[43] and Ube2s[68, 69], but it was unknown whether UBE2C regulates pVHL ubiquitination. Additionally, d-flow was shown to stabilize HIF1α expression under normal atmospheric conditions in vascular endothelial cells by activating NF-KB and inducing expression of the deubiquitinating enzyme Cezanne[42]; however, it was unknown whether pVHL, a well-known HIF1α regulator[38–41], is regulated by flow and regulates HIF1α expression under flow conditions. We found that pVHL is highly flow-sensitive, losing its expression in d-flow in HAVECs and in the fibrosa side exposed to d-flow in a UBE2C-dependent manner. Conversely, d-flow increased HIF1α expression in a UBE2C-dependent manner in HAVECs and in the fibrosa side. These findings suggest that UBE2C regulates pVHL and HIF1α expression in HAVECs. Although there is an increase

in HIF1α expression under d-flow condition, it is interesting to note that siRNA-mediated knockdown of UBE2C is able to significantly reduce the HIF1α expression by post-translational pVHL-mediated degradation preventing the downstream HIF1α signaling cascade.

Mechanistically, we found that UBE2C targets pVHL by binding and mediating its degradation in a ubiquitination-dependent manner. Further, our data using the pVHL ubiquitination site mutants indicates that binding of UBE2C to pVHL is independent of the ubiquitination sites on pVHL; however, the UBE2C-dependent degradation of pVHL requires at least one of its ubiquitination sites. The degradation of pVHL further led to increased stabilization of HIF1α, which in turn induced endothelial inflammation, EndMT and AV calcification (Fig. 7).

To our knowledge, this is the first report showing that UBE2C and pVHL are flow-sensitive proteins and play a role in endothelial inflammation and EndMT. We also found that HIF1α is also flow-sensitive and is a potent pro-inflammatory and pro-EndMT protein in HAVECs. Using the combination of UBE2C, pVHL and HIF1α siRNAs, we found that pVHL and HIF1α mediate the UBE2C-dependent inflammation and EndMT.

Currently, the only treatment option for CAVD patients is AV replacement or repair and there are no effective medical therapies. Therefore, there is an urgent need for developing CAVD therapies[70]. Our study demonstrates that miR-483 and HIF1α-pathway are potential therapeutic targets for CAVD. Treatment with the miR-483 mimic or the HIF1α inhibitor PX478 significantly reduced calcification of porcine AVs in both static and the fibrosa-flow conditions demonstrating their potential as novel anti-CAVD therapeutics. Notably, numerous clinical trials are underway using various HIF1α inhibitors for cancer treatments[71–73]. Our study with PX478 demonstrates the potential of repurposing some of these FDA-approved HIF1α drugs to prevent and treat CAVD. Given our findings, it may be interesting to monitor those patients treated with HIF1α inhibitors for CAVD and atherosclerosis.

While our current *in vitro* studies focus mostly on studying the effect of flow on AV endothelial cells, it is important to note that the expression of UBE2C, pVHL, HIF1α and markers of inflammation, EndMT and AV calcification is regulated in a side-dependent manner *in vivo* as we observed in the human AV tissues. These findings suggest that the miR-483-dependent UBE2C/pVHL/HIF1α pathway established based on the *in vitro* studies is relevant under *in vivo* conditions as well, where AVs are exposed to multiple mechanical forces such as pressure and stretch in addition to flow. A limitation of our *ex vivo* therapeutic studies is that our treatment using the miR-483 mimic or PX478 is not delivered exclusively to the endothelial cells but to the whole AV leaflets [23]. Therefore, the inhibitory effects of the miR-483 mimic or PX478 on AV calcification may not be solely mediated by endothelial cells in the AV leaflets. Whether the effects of the miR-483 mimic or PX478 are mediated by VICs or other cell types in AV remain to be determined.

In conclusion, we identified a flow-sensitive and side-dependent miRNA, miR-483, which targets UBE2C in AV endothelial cells. In turn, the aberrant expression of UBE2C leads to

degradation of pVHL, which increases HIF1α level resulting in endothelial inflammation, EndMT and AV calcification. The miR-483 mimic and HIF1α inhibitor are novel potential CAVD therapeutics.

Supplementary Material

Refer to Web version on PubMed Central for supplementary material.

Acknowledgments:

We acknowledge the many helpful discussions with Jack Heath and Philip Sucosky. HJ is John and Jan Portman Professor and acknowledges the generous support of the late Mr. Portman for the endowed Professorship.

Sources of funding: This work was supported by funding from the National Institutes of Health grants HL119798 and HL095070, and HL113451 to HJ.

Nonstandard Abbreviations and Acronyms

APC/C	anaphase promoting complex/cyclosome
AV	aortic valve
CAVD	calcific aortic valve disease
CTGF	connective tissue growth factor
d-flow	disturbed flow
EC	endotelial cell
ECM	extracelular matrix
EndMT	endothelial-mesenchymal transition
HAVEC	human aortic valve endothelial cell
HEK	human embryonic kidney
HIF1α	hypoxia-inducible factor 1α
ICAM1	intercelular adhesión molecule 1
KLF2	Krüppel-like factor 2
miR-483	microRNA-483–3p
OSI	oscillatory shear index
PAV	porcine aortic valve
pVHL	von Hippel-Lindau tumor suppressor
RUNX2	runt-related transcription factor 2
s-flow	stable flow

TGF-β	transforming growth factor β
UBE2C	ubiquitin E2 ligase C
VCAM1	vascular cell adhesión molecule 1
VEC	valve endothelial cell
VIC	valve interstitial cell

References

1. Otto CM, Lind BK, Kitzman DW, Gersh BJ, Siscovick DS. Association of aortic-valve sclerosis with cardiovascular mortality and morbidity in the elderly. The New England journal of medicine. 1999;341:142–147 [PubMed: 10403851]
2. Hsu SY, Hsieh IC, Chang SH, Wen MS, Hung KC. Aortic valve sclerosis is an echocardiographic indicator of significant coronary disease in patients undergoing diagnostic coronary angiography. International Journal of Clinical Practice. 2005;59:72–77 [PubMed: 15707469]
3. Muneretto C, Alfieri O, Cesana BM, Bisleri G, De Bonis M, Di Bartolomeo R, Savini C, Folesani G, Di Bacco L, Rambaldini M, Maureira JP, Laborde F, Tespili M, Repossini A, Folliguet T. A comparison of conventional surgery, transcatheter aortic valve replacement, and sutureless valves in "real-world" patients with aortic stenosis and intermediate- to high-risk profile. J Thorac Cardiovasc Surg. 2015;150:1570–1577; discussion 1577–1579 [PubMed: 26384753]
4. Dasi LP, Hatoum H, Kheradvar A, Zareian R, Alavi SH, Sun W, Martin C, Pham T, Wang Q, Midha PA, Raghav V, Yoganathan AP. On the mechanics of transcatheter aortic valve replacement. Ann Biomed Eng. 2017;45:310–331 [PubMed: 27873034]
5. Mohler ER, Gannon F, Reynolds C, Zimmerman R, Keane MG, Kaplan FS. Bone formation and inflammation in cardiac valves. Circulation. 2001;103:1522–1528 [PubMed: 11257079]
6. Otto CM, Kuusisto J, Reichenbach DD, Gown AM, Obrien KD. Characterization of the early lesion of degenerative valvular aortic-stenosis - histological and immunohistochemical studies. Circulation. 1994;90:844–853 [PubMed: 7519131]
7. Rajamannan NM, Evans FJ, Aikawa E, Grande-Allen KJ, Demer LL, Heistad DD, Simmons CA, Masters KS, Mathieu P, O'Brien KD, Schoen FJ, Towler DA, Yoganathan AP, Otto CM. Calcific aortic valve disease: Not simply a degenerative process: A review and agenda for research from the national heart and lung and blood institute aortic stenosis working groupexecutive summary: Calcific aortic valve disease – 2011 update. Circulation. 2011;124:1783–1791 [PubMed: 22007101]
8. Schoen FJ. Morphology, clinicopathologic correlations, and mechanisms in heart valve health and disease. Cardiovascular Engineering and Technology. 2018;9:126–140 [PubMed: 27502286]
9. Zhong A, Mirzaei Z, Simmons CA. The roles of matrix stiffness and ß-catenin signaling in endothelial-to-mesenchymal transition of aortic valve endothelial cells. Cardiovascular Engineering and Technology. 2018;9:158–167 [PubMed: 29761409]
10. Dahal S, Huang P, Murray BT, Mahler GJ. Endothelial to mesenchymal transformation is induced by altered extracellular matrix in aortic valve endothelial cells. Journal of Biomedical Materials Research Part A. 2017;105:2729–2741 [PubMed: 28589644]
11. Mahler GJ, Frendl CM, Cao Q, Butcher JT. Effects of shear stress pattern and magnitude on mesenchymal transformation and invasion of aortic valve endothelial cells. Biotechnology and bioengineering. 2014;111:2326–2337 [PubMed: 24898772]
12. Yutzey KE, Demer LL, Body SC, Huggins GS, Towler DA, Giachelli CM, Hofmann-Bowman MA, Mortlock DP, Rogers MB, Sadeghi MM, Aikawa E. Calcific aortic valve disease: A consensus summary from the alliance of investigators on calcific aortic valve disease. Arterioscler Thromb Vasc Biol. 2014;34:2387–2393 [PubMed: 25189570]
13. Fernandez Esmerats J, Heath JM, Jo H. Shear-sensitive genes in aortic valve endothelium. Antioxid Redox Signal. 2015

14. Balachandran K, Sucosky P, Yoganathan AP. Hemodynamics and mechanobiology of aortic valve inflammation and calcification. Int J Inflam. 2011;2011:263870 [PubMed: 21760982]
15. Obrien KD, Reichenbach DD, Marcovina SM, Kuusisto J, Alpers CE, Otto CM. Apolipoproteins b, (a), and e accumulate in the morphologically early lesion of 'degenerative' valvular aortic stenosis. Arterioscler. Thromb. Vasc. Biol 1996;16:523–532 [PubMed: 8624774]
16. Jian B, Jones PL, Li QY, Mohler ER, Schoen FJ, Levy RJ. Matrix metalloproteinase-2 is associated with tenascin-c in calcific aortic stenosis. American Journal of Pathology. 2001;159:321–327 [PubMed: 11438479]
17. Jian B, Narula N, Li QY, Mohler ER, Levy RJ. Progression of aortic valve stenosis: Tgf-beta 1 is present in calcified aortic valve cusps and promotes aortic valve interstitial cell calcification via apoptosis. Annals of Thoracic Surgery. 2003;75:457–465 [PubMed: 12607654]
18. Mohler ER, Chawla MK, Chang AW, Vyavahare N, Levy RJ, Graham L, Gannon FH. Identification and characterization of calcifying valve cells from human and canine aortic valves. Journal of Heart Valve Disease. 1999;8:254–260 [PubMed: 10399657]
19. Cao K, Sucosky P. Computational comparison of regional stress and deformation characteristics in tricuspid and bicuspid aortic valve leaflets. Int J Numer Method Biomed Eng. 2017;33
20. Muller AM, Cronen C, Kupferwasser LI, Oelert H, Muller KM, Kirkpatrick CJ. Expression of endothelial cell adhesion molecules on heart valves: Up-regulation in degeneration as well as acute endocarditis. Journal of Pathology. 2000;191:54–60 [PubMed: 10767719]
21. Ghaisas NK, Foley JB, O'Briain DS, Crean P, Kelleher D, Walsh M. Adhesion molecules in nonrheumatic aortic valve disease: Endothelial expression, serum levels and effects of valve replacement. Journal of the American College of Cardiology. 2000;36:2257–2262 [PubMed: 11127470]
22. Platt MO, Xing Y, Jo H, Yoganathan AP. Cyclic pressure and shear stress regulate matrix metalloproteinases and cathepsin activity in porcine aortic valves. The Journal of heart valve disease. 2006;15:622–629 [PubMed: 17044366]
23. Rathan S, Ankeny CJ, Arjunon S, Ferdous Z, Kumar S, Fernandez Esmerats J, Heath JM, Nerem RM, Yoganathan AP, Jo H. Identification of side- and shear-dependent micrornas regulating porcine aortic valve pathogenesis. Scientific Reports. 2016;6:25397 [PubMed: 27151744]
24. Kumar S, Kim CW, Simmons RD, Jo H. Role of flow-sensitive micrornas in endothelial dysfunction and atherosclerosis: Mechanosensitive athero-mirs. Arteriosclerosis, Thrombosis, and Vascular Biology. 2014;34:2206–2216
25. Tarbell JM, Shi ZD, Dunn J, Jo H. Fluid mechanics, arterial disease, and gene expression. Annual review of fluid mechanics. 2014;46:591–614
26. Kwak BR, Bäck M, Bochaton-Piallat M-L, Caligiuri G, Daemen MJ, Davies PF, Hoefer IE, Holvoet P, Jo H, Krams R. Biomechanical factors in atherosclerosis: Mechanisms and clinical implications. European heart journal. 2014:ehu353
27. Holliday CJ, Ankeny RF, Jo H, Nerem RM. Discovery of shear- and side-specific mrnas and mirnas in human aortic valvular endothelial cells. Am J Physiol Heart Circ Physiol. 2011;301:H856–867 [PubMed: 21705672]
28. Heath JM, Fernandez Esmerats J, Khambouneheuang L, Kumar S, Simmons RD, Jo H. Mechanosensitive microrna-181b regulates aortic valve endothelial matrix degradation by targeting timp3. Cardiovacular Engineering and Technology. 2017
29. He M, Chen Z, Martin M, Zhang J, Sangwung P, Woo B, Tremoulet AH, Shimizu C, Jain MK, Burns JC, Shyy JY. Mir-483 targeting of ctgf suppresses endothelial-to-mesenchymal transition: Therapeutic implications in kawasaki disease. Circ Res. 2017;120:354–365 [PubMed: 27923814]
30. Kemp JR, Unal H, Desnoyer R, Yue H, Bhatnagar A, Karnik SS. Angiotensin ii-regulated microrna 483–3p directly targets multiple components of the renin-angiotensin system. Journal of molecular and cellular cardiology. 2014;75:25–39 [PubMed: 24976017]
31. Garbacki N, Di Valentin E, Huynh-Thu VA, Geurts P, Irrthum A, Crahay C, Arnould T, Deroanne C, Piette J, Cataldo D, Colige A. Micrornas profiling in murine models of acute and chronic asthma: A relationship with mrnas targets. PLOS ONE. 2011;6:e16509 [PubMed: 21305051]
32. Takahashi Y, Ishii Y, Nishida Y, Ikarashi M, Nagata T, Nakamura T, Yamamori S, Asai S. Detection of aberrations of ubiquitin-conjugating enzyme e2c gene (ube2c) in advanced colon

cancer with liver metastases by DNA microarray and two-color fish. Cancer Genetics and Cytogenetics.168:30–35 [PubMed: 16772118]

33. Hao Z, Zhang H, Cowell J. Ubiquitin-conjugating enzyme ube2c: Molecular biology, role in tumorigenesis, and potential as a biomarker. Tumor Biology. 2012;33:723–730 [PubMed: 22170434]
34. Morikawa T, Kawai T, Abe H, Kume H, Homma Y, Fukayama M. Ube2c is a marker of unfavorable prognosis in bladder cancer after radical cystectomy. International Journal of Clinical and Experimental Pathology. 2013;6:1367–1374 [PubMed: 23826418]
35. Chou C-P, Huang N-C, Jhuang S-J, Pan H-B, Peng N-J, Cheng J-T, Chen C-F, Chen J-J, Chang T-H. Ubiquitin-conjugating enzyme ube2c is highly expressed in breast microcalcification lesions. PLOS ONE. 2014;9:e93934 [PubMed: 24699941]
36. Kim WT, Jeong P, Yan C, Kim YH, Lee I-S, Kang H-W, Kim Y-J, Lee S-C, Kim SJ, Kim YT, Moon S-K, Choi Y-H, Kim IY, Yun SJ, Kim W-J. Ube2c cell-free rna in urine can discriminate between bladder cancer and hematuria. Oncotarget. 2016;7:58193–58202 [PubMed: 27528424]
37. Somers P, Knaapen M, Kockx M, van Cauwelaert P, Bortier H, Mistiaen W. Histological evaluation of autophagic cell death in calcified aortic valve stenosis. The Journal of heart valve disease. 2006;15:43–47; discussion 48 [PubMed: 16480011]
38. Maxwell PH, Pugh CW, Ratcliffe PJ. The pvhl-hif-1 system. A key mediator of oxygen homeostasis. Adv Exp Med Biol. 2001;502:365–376 [PubMed: 11950150]
39. Semenza GL. Targeting hif-1 for cancer therapy. Nature reviews Cancer. 2003;3:721–732 [PubMed: 13130303]
40. Gao L, Chen Q, Zhou X, Fan L. The role of hypoxia-inducible factor 1 in atherosclerosis. J Clin Pathol. 2012;65:872–876 [PubMed: 22569539]
41. Majmundar AJ, Wong WJ, Simon MC. Hypoxia-inducible factors and the response to hypoxic stress. Mol Cell. 2010;40:294–309 [PubMed: 20965423]
42. Feng S, Bowden N, Fragiadaki M, Souilhol C, Hsiao S, Mahmoud M, Allen S, Pirri D, Ayllon BT, Akhtar S, Thompson AAR, Jo H, Weber C, Ridger V, Schober A, Evans PC. Mechanical activation of hypoxia-inducible factor 1α drives endothelial dysfunction at atheroprone sites. Arteriosclerosis, Thrombosis, and Vascular Biology. 2017;37:2087–2101
43. Liu W, Xin H, Eckert DT, Brown JA, Gnarra JR. Hypoxia and cell cycle regulation of the von hippel-lindau tumor suppressor. Oncogene. 2011;30:21–31 [PubMed: 20802534]
44. Ankeny RF, Thourani VH, Weiss D, Vega JD, Taylor WR, Nerem RM, Jo H. Preferential activation of smad1/5/8 on the fibrosa endothelium in calcified human aortic valves - association with low bmp antagonists and smad6. PLoS ONE. 2011;6:e20969 [PubMed: 21698246]
45. Dewey CF, Jr., Bussolari SR, Gimbrone MA, Jr., Davies PF. The dynamic response of vascular endothelial cells to fluid shear stress. J Biomech Eng. 1981;103:177–185 [PubMed: 7278196]
46. Go YM, Boo YC, Park H, Maland MC, Patel R, Pritchard KA, Jr., Fujio Y, Walsh K, Darley-Usmar V, Jo H. Protein kinase b/akt activates c-jun nh(2)-terminal kinase by increasing no production in response to shear stress. J Appl Physiol (1985). 2001;91:1574–1581 [PubMed: 11568138]
47. Balachandran K, Sucosky P, Jo H, Yoganathan AP. Elevated cyclic stretch induces aortic valve calcification in a bone morphogenic protein-dependent manner. The American journal of pathology. 2010;177:49–57 [PubMed: 20489151]
48. Sucosky P, Padala M, Elhammali A, Balachandran K, Jo H, Yoganathan AP. Design of an ex vivo culture system to investigate the effects of shear stress on cardiovascular tissue. Journal of Biomechanical Engineering. 2008;130:035001–035001 [PubMed: 18532871]
49. Sucosky P, Balachandran K, Elhammali A, Jo H, Yoganathan A. Altered shear stress stimulates upregulation of endothelial vcam-1 and icam-1 in a bmp-4- and tgf-beta1-dependent pathway. Arterioscler Thromb Vasc Biol. 2009;29:254–260 [PubMed: 19023092]
50. Sucosky P, Balachandran K, Elhammali A, Jo H, Yoganathan AP. Altered shear stress stimulates upregulation of endothelial vcam-1 and icam-1 in a bmp-4– and tgf-β1–dependent pathway. Arteriosclerosis, Thrombosis, and Vascular Biology. 2009;29:254–260
51. Ni CW, Qiu H, Jo H. Microrna-663 upregulated by oscillatory shear stress plays a role in inflammatory response of endothelial cells. Am J Physiol Heart Circ Physiol. 2011;300:H1762–1769 [PubMed: 21378144]

52. Metcalf JL, Bradshaw PS, Komosa M, Greer SN, Stephen Meyn M, Ohh M. K63-ubiquitylation of vhl by socs1 mediates DNA double-strand break repair. Oncogene. 2014;33:1055–1065 [PubMed: 23455319]
53. Stickle NH, Chung J, Klco JM, Hill RP, Kaelin WG, Jr., Ohh M Pvhl modification by nedd8 is required for fibronectin matrix assembly and suppression of tumor development. Mol Cell Biol. 2004;24:3251–3261 [PubMed: 15060148]
54. Wang Y, Sun H-Y, Kumar S, Puerta MdM, Jo H, Rezvan A. Zbtb46 is a shear-sensitive transcription factor inhibiting endothelial cell proliferation via gene expression regulation of cell cycle proteins. Laboratory Investigation. 2018
55. Tressel SL, Huang R-P, Tomsen N, Jo H. Laminar shear inhibits tubule formation and migration of endothelial cells by an angiopoietin-2 dependent mechanism. Arteriosclerosis, thrombosis, and vascular biology. 2007;27:2150–2156
56. Mahler GJ, Farrar EJ, Butcher JT. Inflammatory cytokines promote mesenchymal transformation in embryonic and adult valve endothelial cells. Arteriosclerosis, Thrombosis, and Vascular Biology. 2013;33:121–130
57. Lee J-W, Bae S-H, Jeong J-W, Kim S-H, Kim K-W. Hypoxia-inducible factor (hif-1)[alpha]: Its protein stability and biological functions. Exp Mol Med. 0000;36:1–12 [PubMed: 15031665]
58. Bertero T, Bourget-Ponzio I, Puissant A, Loubat A, Mari B, Meneguzzi G, Auberger P, Barbry P, Ponzio G, Rezzonico R. Tumor suppressor function of mir-483–3p on squamous cell carcinomas due to its pro-apoptotic properties. Cell Cycle. 2013;12:2183–2193 [PubMed: 24067364]
59. Bertero T, Gastaldi C, Bourget-Ponzio I, Mari B, Meneguzzi G, Barbry P, Ponzio G, Rezzonico R. Cdc25a targeting by mir-483–3p decreases ccnd-cdk4/6 assembly and contributes to cell cycle arrest. Cell Death Differ. 2013;20:800–811 [PubMed: 23429262]
60. Lupini L, Pepe F, Ferracin M, Braconi C, Callegari E, Pagotto S, Spizzo R, Zagatti B, Lanuti P, Fornari F, Ghasemi R, Mariani-Costantini R, Bolondi L, Gramantieri L, Calin GA, Sabbioni S, Visone R, Veronese A, Negrini M. Over-expression of the mir-483–3p overcomes the mir-145/tp53 pro-apoptotic loop in hepatocellular carcinoma. Oncotarget. 2016
61. Pepe F, Pagotto S, Soliman S, Rossi C, Lanuti P, Braconi C, Mariani-Costantini R, Visone R, Veronese A. Regulation of mir-483–3p by the o-linked n-acetylglucosamine transferase links chemosensitivity to glucose metabolism in liver cancer cells. Oncogenesis. 2017;6:e328 [PubMed: 28481368]
62. Rathan S, Ankeny CJ, Arjunon S, Ferdous Z, Kumar S, Fernandez Esmerats J, Heath JM, Nerem RM, Yoganathan AP, Jo H. Identification of side- and shear-dependent micrornas regulating porcine aortic valve pathogenesis. Sci Rep. 2016;6:25397 [PubMed: 27151744]
63. Penas C, Ramachandran V, Ayad N. The apc/c ubiquitin ligase: From cell biology to tumorigenesis. Frontiers in Oncology. 2012;1
64. Zhou Z, He M, Shah AA, Wan Y. Insights into apc/c: From cellular function to diseases and therapeutics. Cell Division. 2016;11:9 [PubMed: 27418942]
65. McLean JR, Chaix D, Ohi MD, Gould KL. State of the apc/c: Organization, function, and structure. Critical reviews in biochemistry and molecular biology. 2011;46:118–136 [PubMed: 21261459]
66. Bavi P, Uddin S, Ahmed M, Jehan Z, Bu R, Abubaker J, Sultana M, Al-Sanea N, Abduljabbar A, Ashari LH, Alhomoud S, Al-Dayel F, Prabhakaran S, Hussain AR, Al-Kuraya KS. Bortezomib stabilizes mitotic cyclins and prevents cell cycle progression via inhibition of ube2c in colorectal carcinoma. The American journal of pathology. 2011;178:2109–2120 [PubMed: 21514426]
67. Lin J, Raoof DA, Wang Z, Lin MY, Thomas DG, Greenson JK, Giordano TJ, Orringer MB, Chang AC, Beer DG, Lin L. Expression and effect of inhibition of the ubiquitin-conjugating enzyme e2c on esophageal adenocarcinoma. Neoplasia. 2006;8:1062–1071 [PubMed: 17217624]
68. Jung C-R, Hwang K-S, Yoo J, Cho W-K, Kim J-M, Kim WH, Im D-S. E2-epf ucp targets pvhl for degradation and associates with tumor growth and metastasis. Nature medicine. 2006;12:809–816
69. Park K-S, Kim JH, Shin HW, Chung K-S, Im D-S, Lim JH, Jung C-R. E2-epf ucp regulates stability and functions of missense mutant pvhl via ubiquitin mediated proteolysis. BMC Cancer. 2015;15:800 [PubMed: 26503325]

70. Choi B, Lee S, Kim SM, Lee EJ, Lee SR, Kim DH, Jang JY, Kang SW, Lee KU, Chang EJ, Song JK. Dipeptidyl peptidase-4 induces aortic valve calcification by inhibiting insulin-like growth factor-1 signaling in valvular interstitial cells. Circulation. 2017;135:1935–1950 [PubMed: 28179397]

71. Yu T, Tang B, Sun X. Development of inhibitors targeting hypoxia-inducible factor 1 and 2 for cancer therapy. Yonsei Medical Journal. 2017;58:489–496 [PubMed: 28332352]

72. Eltzschig HK, Bratton DL, Colgan SP. Targeting hypoxia signalling for the treatment of ischaemic and inflammatory diseases. Nature reviews. Drug discovery. 2014;13:852–869 [PubMed: 25359381]

73. Diaz-Gonzalez JA, Russell J, Rouzaut A, Gil-Bazo I, Montuenga L. Targeting hypoxia and angiogenesis through hif-1alpha inhibition. Cancer Biol Ther. 2005;4:1055–1062 [PubMed: 16294030]

Highlights

- We identified miR-483, UBE2C, pVHL and HIF1α as novel flow-sensitive and side-specific genes and proteins in AV leaflets.
- miR-483 directly targets UBE2C, which in turn mediates flow-induced AV endothelial inflammation and EndMT.
- We found that pVHL is a novel substrate of UBE2C. Ubiquitination and degradation of pVHL by UBE2C leads to HIF1α stabilization, a novel mechanism.
- Staining studies with human AV leaflets demonstrate the side-specific expression of the flow-sensitive molecules as observed in our *in vitro* studies: the fibrosa-side (naturally exposed to OS) shows increased UBE2C and HIF1α expression, while pVHL expression is higher in the ventricularis-side (naturally exposed to s-flow).
- The miR-483 mimic and HIF1α inhibitor (PX478) inhibit AV calcification and are potential therapeutics for CAVD.

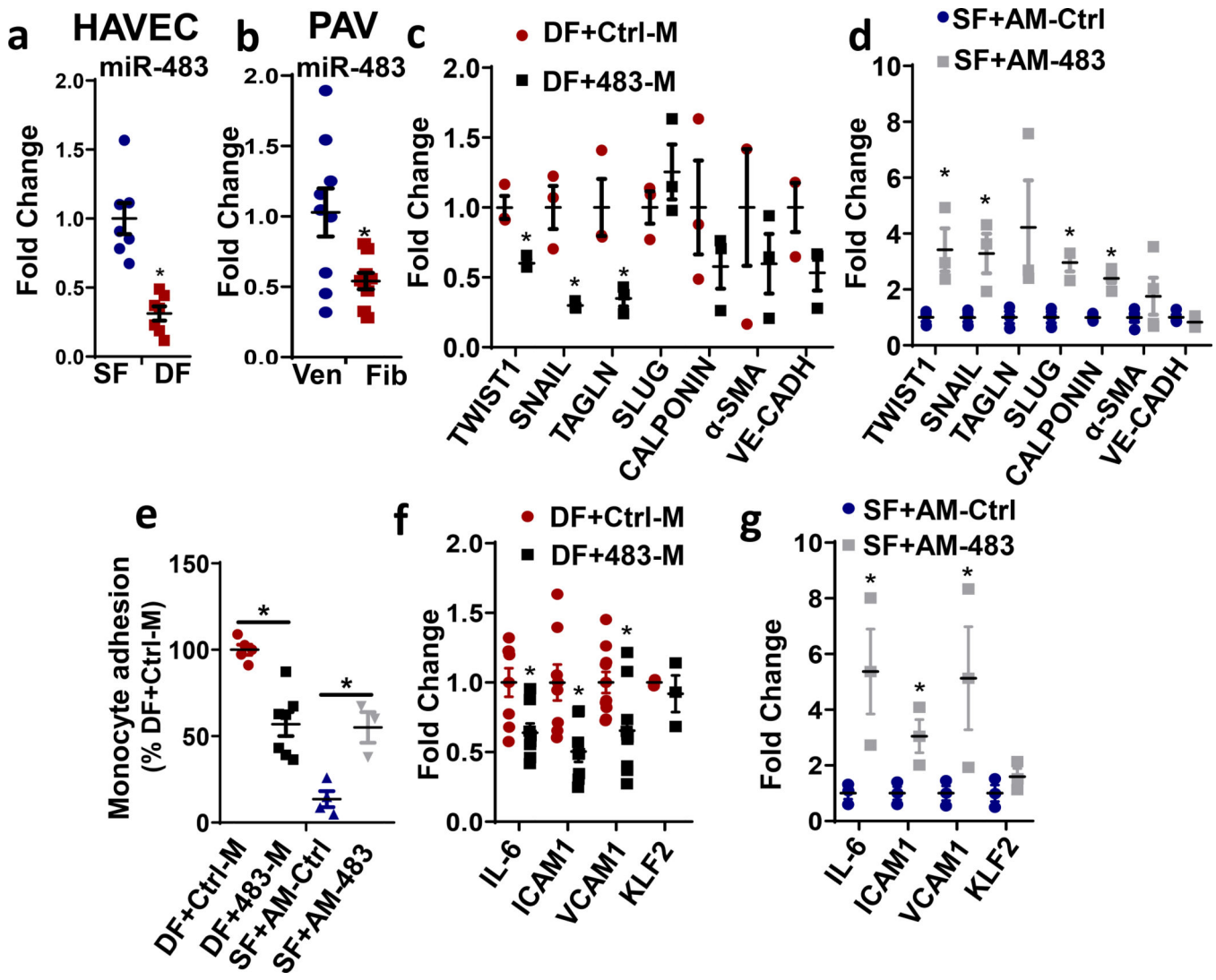

Figure 1. miR-483 expression is shear-sensitive and side-specific in ECs, and regulates shear-dependent EndMT and inflammation.

a,b) miR-483 qPCR was performed using **a**) RNAs from HAVECs exposed to unidirectional laminar (SF) or oscillatory shear (DF) for 24 hours (n=7) and **b**) endothelial-enriched total RNA from the ventricularis (Ven) and the fibrosa (Fib) side of healthy porcine AVs normalized to U6 (n=9). **c**-**g**) HAVECs transfected with miR-483 mimic (483-M), control mimic (Ctrl-M), anti-miR-483 (AM-483) or Anti-miR scramble (AM-Ctrl) for 24 hours were exposed to d-flow (DF) or s-flow (SF) for 24 hours. Following shear, total RNAs were prepared for qPCR to analyze markers of EndMT (n=3–4) (**c,d**) and inflammation (n=3–7) (**f,g**) normalized to 18S, or cells were used for THP1 monocyte adhesion assay (n=3–7) (**e**). Mean±sem, *p<0.05.

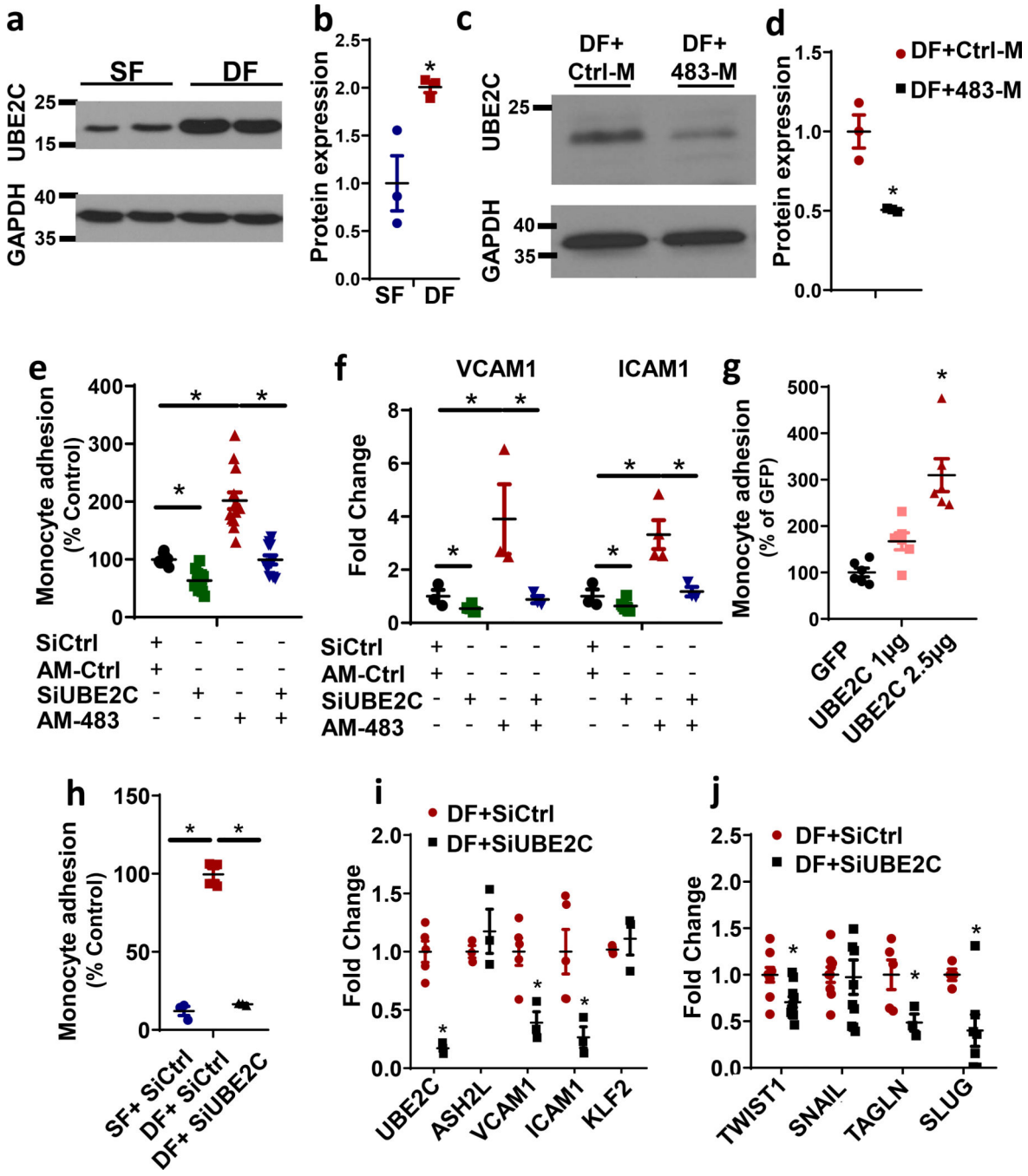

Figure 2. UBE2C is a shear-dependent target of miR-483 and regulates DF- and miR-483-induced inflammation and EndMT in HAVECs.

a,b) UBE2C expression was increased in HAVECs exposed to d-flow (DF) compared to s-flow (SF) for 24 hours, as determined by Western blot and its quantification by ImageJ (n=3). **c,d**) HAVECs treated with miR-483-mimic (483-M) or control mimic (Ctrl-M) followed by DF were analyzed by UBE2C Western blot and its quantification (n=3). **e-g**) HAVECs were co-transfected with siUBE2C or siCtrl and anti-miR-483 (AM-483) or anti-miR-control (AM-Ctrl), followed by monocyte adhesion (n=11) (**e**) and qPCR analysis for

inflammatory markers (n=3) (**f**). **g**) HAVECs transfected with UBE2C overexpression plasmid or GFP plasmid were used for monocyte adhesion assay (n=6). **h-i**) HAVECs treated with siUBE2C or siRNA control (SiCtrl) for 24 hours, followed by DF or SF conditions for another 24 hours. Then, monocyte adhesion (**h**) and qPCR analyses for markers of inflammation (**i**) and EndMT (**j**) were carried out, normalized to 18S (n=4–6). Mean±sem, *$p<0.05$.

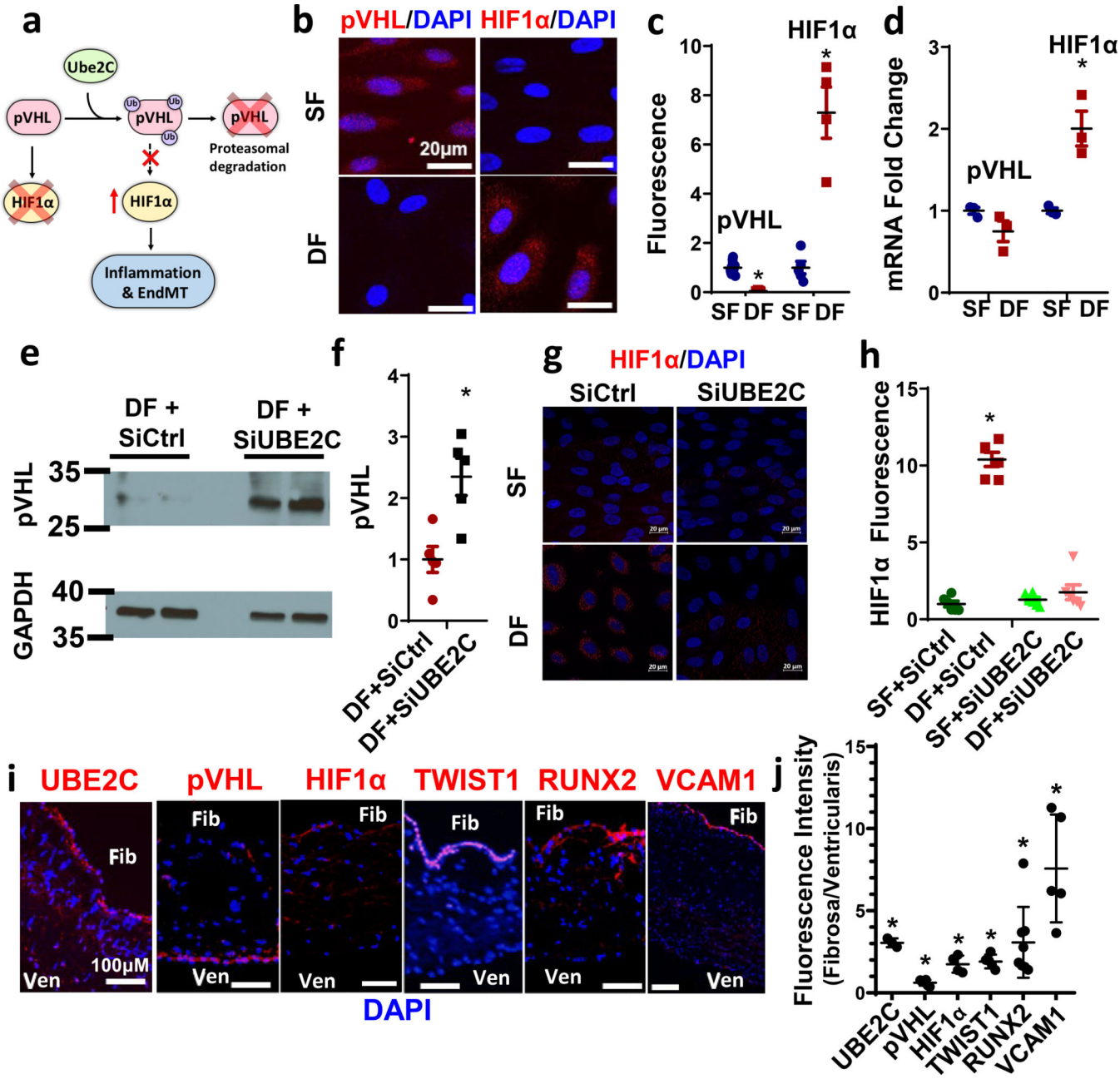

Figure 3. UBE2C mediates shear-dependent expression of pVHL and HIF1α in HAVECs, and UBE2C, pVHL and HIF1α are expressed in a side-dependent manner in human AV leaflets.

a) Depicts a hypothesis that overexpression of UBE2C ubiquitinates pVHL, leading to increased HIF1α level, endothelial inflammation and EndMT. **b)** HAVECs sheared for 72 hours by s-flow (SF) or d-flow (DF) were immunostained with antibodies for pVHL or HIF1α (**b**) and quantification of the image was done using ImageJ (**c**), or by qPCR (**d**) normalized to 18S (n=3–4). **e**) HAVECs treated with siCtrl or siUBE2C for 24 hours, followed by exposure to DF for 24 hours, were analyzed by Western blot (**e**) and Image J quantification (**f**) for pVHL (n=5). For the HIF1α study, HAVECs exposed to DF for 72 hours were immunostained with HIF1α (**g**) and Image J quantified (**h**) (n=6). **i**) Human AVs

with sclerosis were stained with antibodies to UBE2C, pVHL, HIF1α, Twist1 and Runx2 with DAPI nuclear staining, and **j**) shows quantification of the fluorescent intensities of each staining in the endothelial layer on each side using Image J (n=5–8). Mean±sem, *p<0.05. F: fibrosa, V: ventricularis.

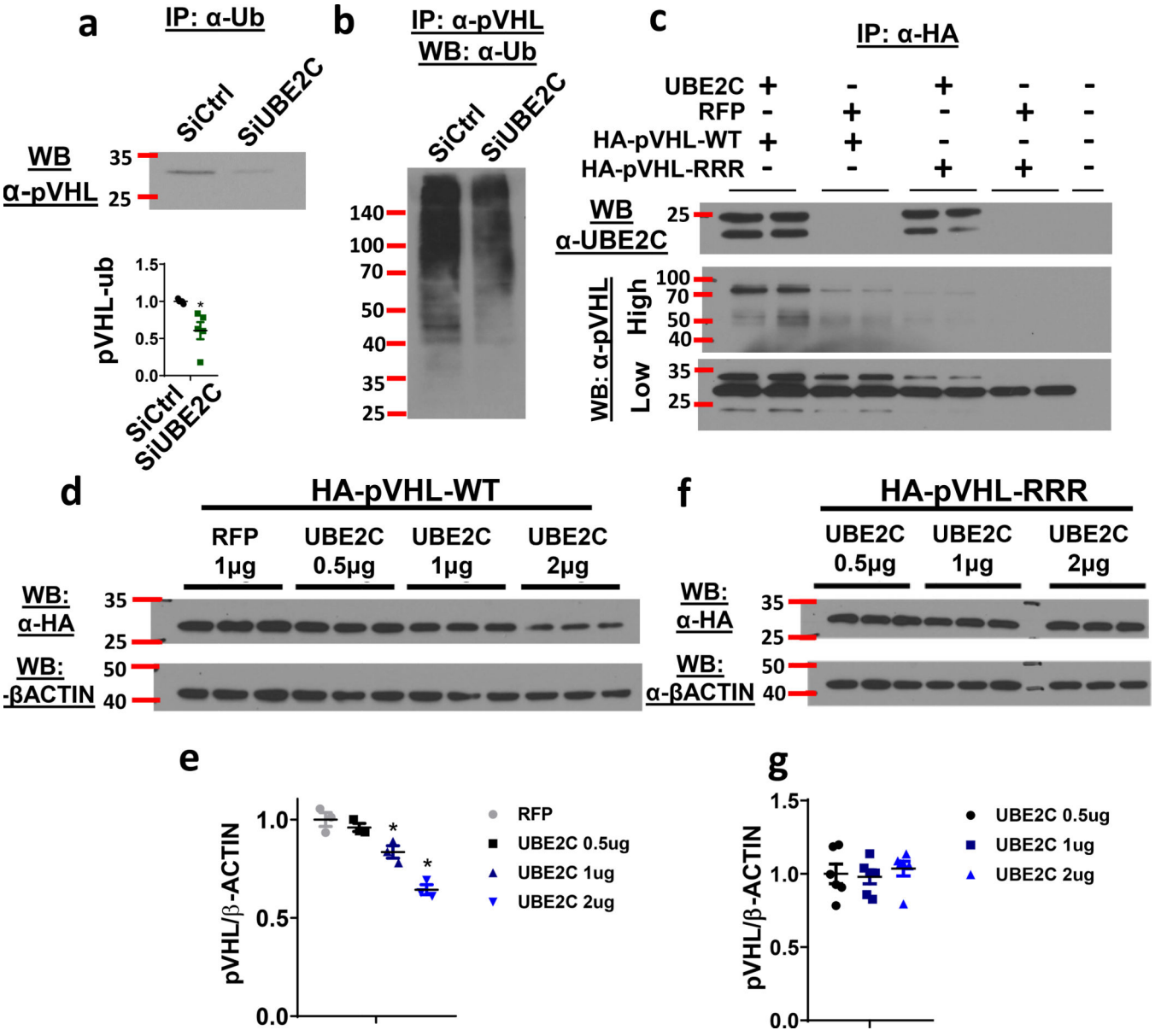

Figure 4. UBE2C binds and ubiquitinates pVHL, leading to its degradation.

a,b) HAVECs transfected with siUBE2C or siCtrl were immunoprecipitated with an antibody for ubiquitin (Ub) (**a**) or pVHL (**b**) and Western blotted with the pVHL (**a**) or Ub (**b**) antibody (n=5). **c)** HEK cells co-transfected with myc-UBE2C or RFP plasmid (1µg) and HA-pVHL-WT or HA-pVHL-RRR mutant plasmids (0.5µg) for 48 hours were immunoprecipitated using the antibody to HA-tag and Western blotted with the antibody to UBE2C or pVHL (exposed using High-intensity ECL and Low-intensity ECL). Untreated (Unt) HEK cells were used as a control. **d-g**) HEK cells co-transfected with HA-pVHL-WT or HA-pVHL-RRR mutant plasmids and increasing doses of UBE2C (0.5–2µg) or RFP plasmids for 48 hours were lysed and Western blotted with antibodies to pVHL and β-actin as an internal control (**d,f**), and ImageJ quantified (**e,g**) (n=3–6). Mean±sem, *p<0.05.

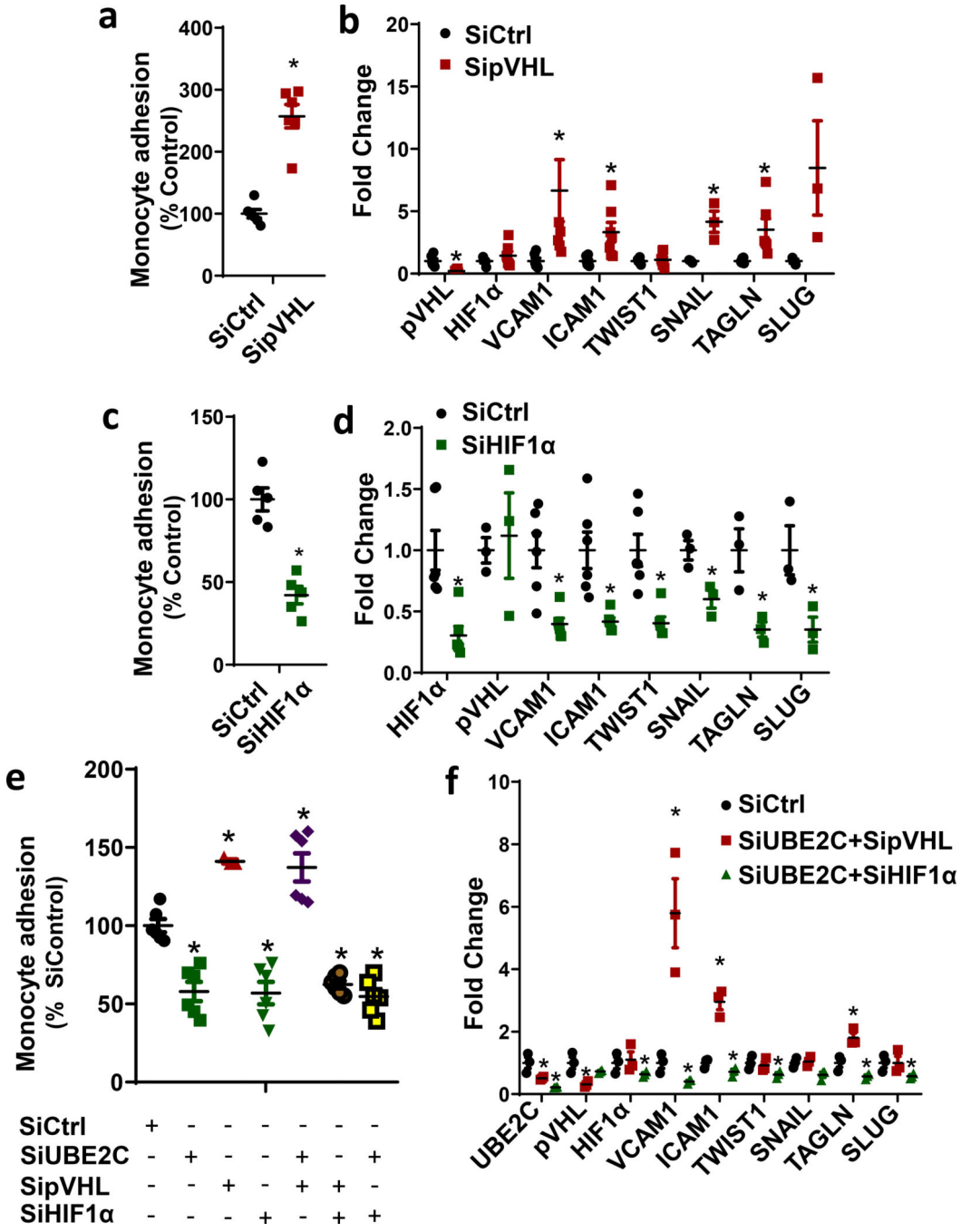

Figure 5. pVHL and HIF1α mediate UBE2C-induced endothelial inflammation and EndMT.

a,b) HAVECs were transfected either individually with sipVHL, siHIF1α, and siCtrl (**a-d**) or co-transfected with siUBE2C (**e,f**) for 48 hours. Treated cells were then used for monocyte adhesion assay (**a,c,e**) or qPCR analyses for markers of inflammation and EndMT (**b,d,f**) normalized to 18S (n=3–6). Mean±sem. *p<0.05.

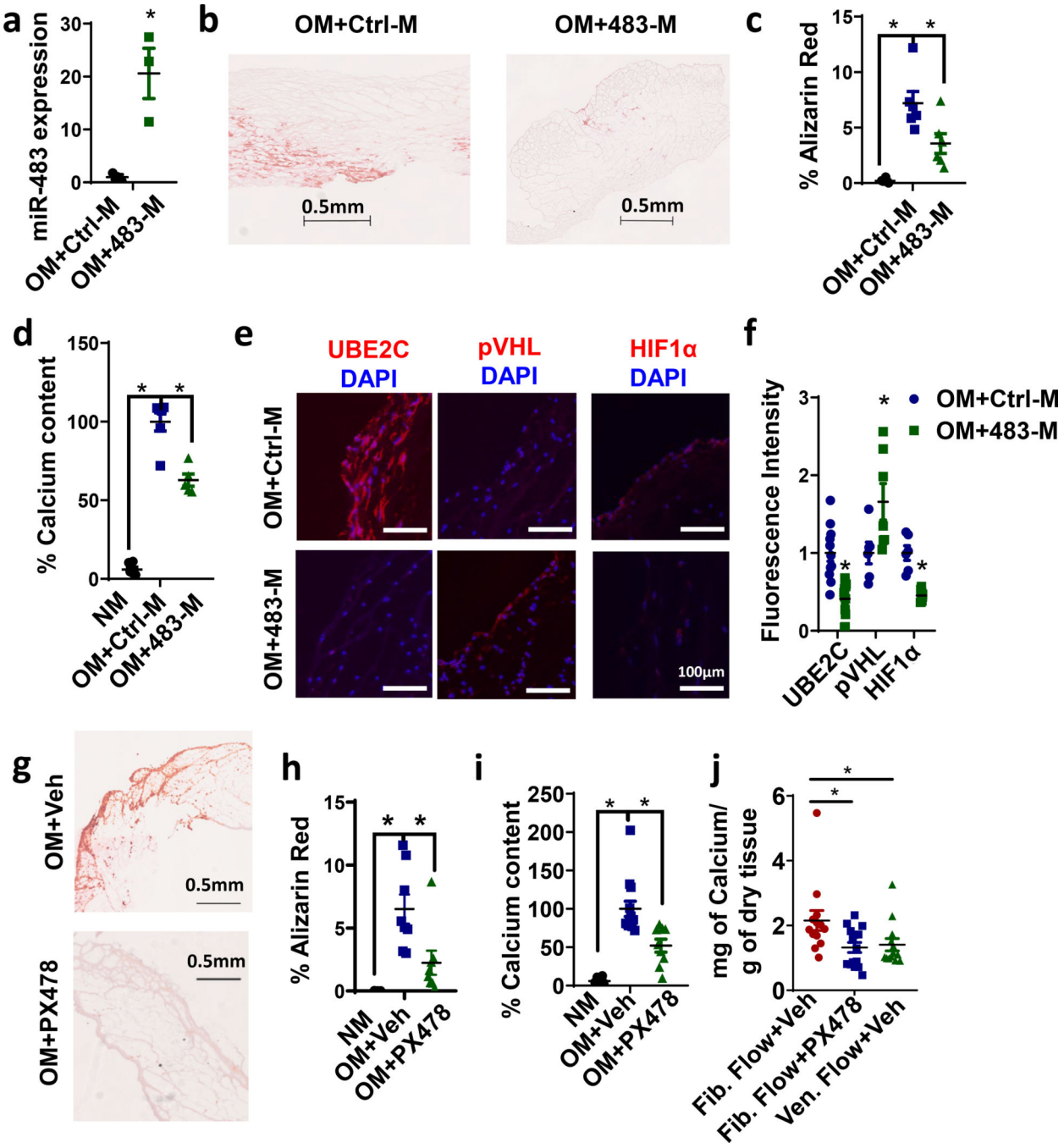

Figure 6. The miR-483-mimic or HIF1α inhibitor inhibits AV calcification.

a) Freshly-harvested porcine AV leaflets were transfected with either miR-483 mimic or Ctrl mimic (**a-f**) or PX478 (20 μM) or HBSS vehicle (**g-i**) every 3 days for 2 weeks in osteogenic media (OM). AV leaflets were then divided for total RNA isolation and qPCR assay for miR-483 (**a**) (n=3), immunohistochemical assay using Alizarin Red (**b,c**) (n=6) and antibodies for UBE2C, pVHL and HIF1α (**e,f**) (n=6–12) and Arsenazo calcium assay (**d**) (n=5–6). Alizarin images were quantified using MATLAB (**c,h**) while the fluorescence images (**e**) were quantified by ImageJ (n=3–12). **j)** Porcine AV leaflets were exposed to

fibrosa-(Fib.) or ventricularis-(Ven.) flow profiles in osteogenic media for 7 days with PX478 (20μM) or vehicle. Total calcium was quantified via Arsenazo assay and normalized to dry tissue weight (n=13–15). Mean±sem, *p<0.05.

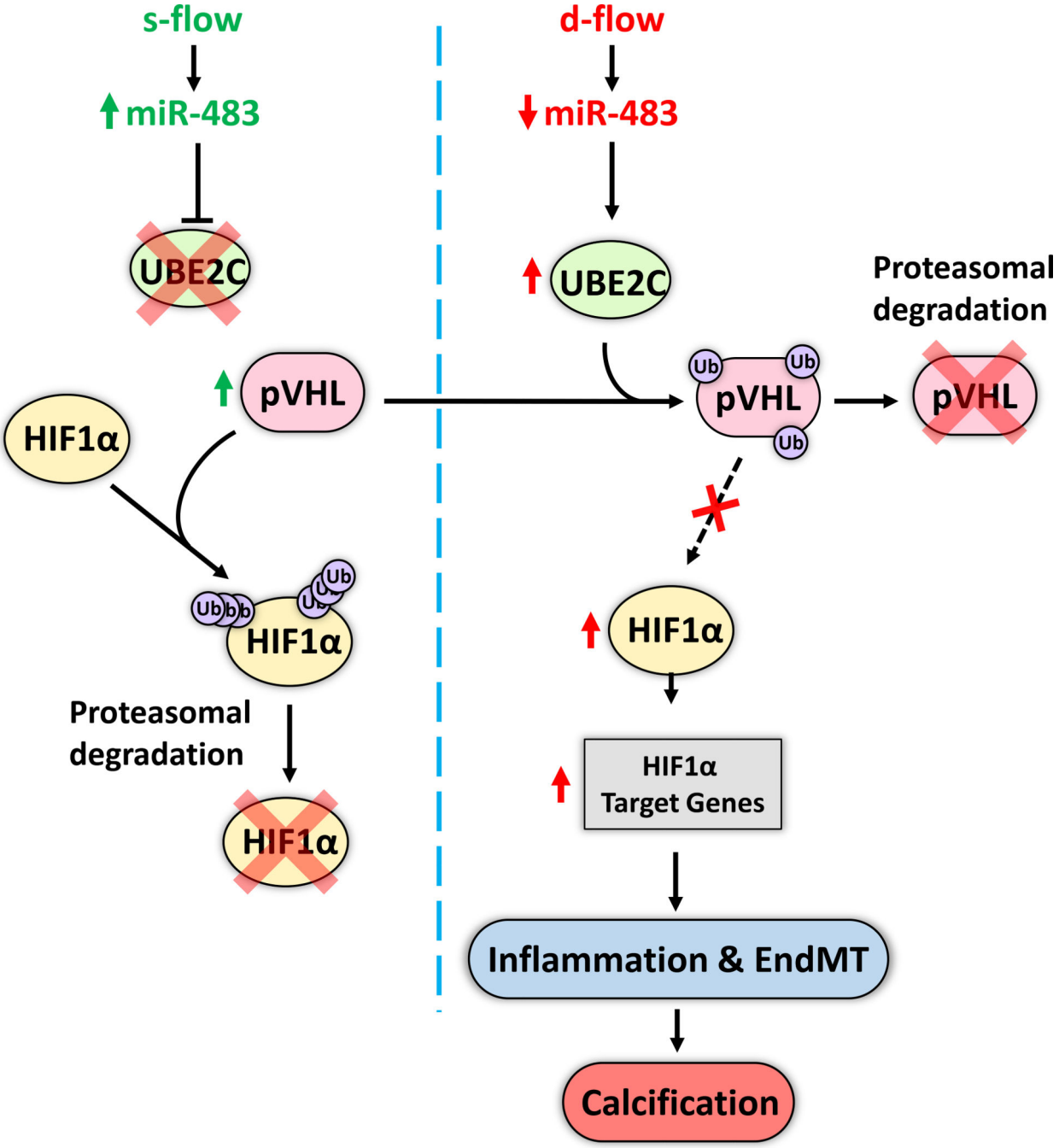

Figure 7. Working hypothesis